Magazine of Concrete Research, 2010, **62**, No. 4, April, 301–311
doi: 10.1680/macr.2010.62.4.301

RC beams shear-strengthened with FRP: shear resistance contributed by FRP

G. M. Chen*, J. G. Teng* and J. F. Chen†

Hong Kong Polytechnic University; University of Edinburgh

In determining the shear strength of reinforced concrete (RC) beams shear-strengthened with externally bonded fibre-reinforced polymer (FRP) reinforcement, the evaluation of the shear resistance contributed by the FRP reinforcement is the key issue. When the FRP reinforcement is in the form of U-jackets or side strips, debonding of the FRP reinforcement from the concrete substrate generally governs the shear strength of the beam and the evaluation of the shear resistance from the FRP becomes more challenging. In this paper, a theoretical shear strength model in closed-form expressions modified from a model proposed by Chen and Teng for shear debonding failure is first presented. A computational model that captures the debonding process more accurately than the closed-form theoretical model is then described. Predictions from both the original model of Chen and Teng and the modified theoretical model are then compared with results from the computational model. These numerical comparisons show that Chen and Teng's original model provides closer predictions for the shear resistance contributed by FRP side strips, but the modified theoretical model generally leads to slightly more accurate predictions for FRP U-jackets. The reasons behind this are explained. The original model of Chen and Teng is recommended as the more suitable model for use in design, given its overall accuracy and simpler form.

Notation

C	shear crack shape factor
D_{frp}	stress distribution factor for FRP strips intersected by the critical shear crack
d	distance from beam compression face to centroid of steel tension reinforcement
E_{f}	modulus of elasticity of FRP
$\boldsymbol{f}'_{\text{c}}$	concrete cylinder compressive strength
$\boldsymbol{f}_{\text{fu}}$	tensile strength of FRP
$\boldsymbol{f}_{\text{f,e}}$	average/effective stress of FRP strips intersected by the critical shear crack
h	height of beam
h_{f}	effective height of FRP strips
h_{t}	vertical distance from tip of critical shear crack to top edge of FRP
h_{b}	vertical distance from end of critical shear crack to lower edge of FRP
L_{max}	maximum bond length of FRP strips intersected by the critical shear crack
L_{e}	effective bond length of FRP strips
s_{f}	centre-to-centre spacing of FRP strips measured along the longitudinal axis
t_{f}	thickness of FRP strips
V_{c}	contribution of concrete to shear capacity
V	contribution of shear strengthening FRP strips to shear capacity
V_{s}	contribution of steel shear reinforcement to shear capacity
V_{u}	shear capacity of shear-strengthened beam
w_{f}	width of individual FRP strips (perpendicular to the fibre orientation)
z	vertical co-ordinate starting from tip of critical shear crack
z_{b}	vertical co-ordinate of end of critical shear crack
$\bar{z}$	normalized vertical co-ordinate
β	angle of fibre orientation measured clockwise from the longitudinal axis of a beam
β_{L}	FRP bond length coefficient
β_{w}	FRP strip width coefficient
λ	normalized FRP maximum bond length
λ_0	normalized bond length (i.e. $h_{f,e}/\sin\beta$) of FRP strips within the effective bonded area

* Department of Civil and Structural Engineering, The Hong Kong Polytechnic University, Hong Kong, China
† Institute of Infrastructure and Environment, Joint Research Institute for Civil and Environmental Engineering, School of Engineering, The University of Edinburgh, Edinburgh, UK

(MACR 900039) Paper received 24 February 2009; accepted 5 August 2009

www.concrete-research.com 1751-763X (Online) 0024-9831 (Print)

λ_1 normalized bond length of FRP strips above the effective bonded area
λ_2 normalized bond length of FRP strips below the effective bonded area
θ angle of critical shear crack to the longitudinal axis of a beam
$\sigma_{f,max}$ maximum stress in FRP strips intersected by the critical shear crack
$\sigma_{f,z}$ stress in FRP where the intersecting shear crack is at the vertical coordinate z

Introduction

External bonding of fibre-reinforced polymer (FRP) composites has become a popular technique for strengthening reinforced concrete (RC) structures in the past two decades (Hollaway and Teng, 2008; Teng *et al.*, 2002). Owing to the complex nature of the shear failure process, the behaviour of RC beams shear-strengthened with FRP is still not well understood (Bousselham and Chaallal, 2004, 2008; Teng *et al.*, 2004). The externally bonded FRP reinforcement can take various configurations (Chen and Teng, 2003a), but in the present paper the FRP reinforcement is assumed to be in the form of evenly distributed discrete vertical strips of identical width with vertical fibres only for simplicity of discussion unless otherwise stated. Such strips may be bonded around the entire cross-section of the beam (i.e. full wraps), as U-jackets covering the tension face and the two side faces, and to the side faces only (i.e. side strips). Continuous FRP sheets can be treated as a special case of discrete FRP strips where the clear distances between strips are zero.

Much research has been conducted on the shear strengthening of RC beams with FRP, but the majority of these studies have been experimental (Bousselham and Chaallal, 2006; Cao *et al.*, 2005; Carolin and Taljsten, 2005a; Khalifa and Nanni, 2002; Leung *et al.*, 2007; Li *et al.* 2002; Teng *et al.*, 2009) and fewer studies have taken a theoretical approach (Chen and Teng, 2003a, 2003b; Colotti *et al.*, 2004; Deniaud and Cheng, 2004). Existing studies have led to the development of a number of shear strength models for FRP-strengthened RC beams for design use (Carolin and Taljsten, 2005b; Chaallal *et al.*, 1998; Chen and Teng, 2003a, 2003b; Khalifa *et al.*, 1998; Triantafillou, 1998; Triantafillou and Antonopoulos, 2000; Taljsten, 2003). In these models, the shear resistance of the strengthened beam V_u is assumed to be the sum of the contributions from the concrete V_c, the steel shear reinforcement (only stirrups are considered in this paper for ease of discussion) V_s, and the externally bonded FRP reinforcement V_f. That is

$$V_u = V_c + V_s + V_f \quad (1)$$

In such shear strength models, V_c and V_s are generally evaluated using existing design codes, implying that all steel stirrups intersected by the critical shear crack are assumed to reach their yield strength at beam shear failure. The main differences between the different shear strength models available therefore lie in how the FRP contribution V_f to the beam shear resistance is evaluated. It should be noted that these three components (i.e. V_c, V_s and V_f) are not strictly independent (Teng *et al.*, 2009), so Equation 1 is only an engineering approximation of reality. Nevertheless, Equation 1 has the advantage of simplicity so it has been widely accepted.

In evaluating the shear resistance from the FRP reinforcement, it is important to note that owing to the linear-elastic-brittle behaviour of FRP and the non-uniform strain distribution in the FRP reinforcement in a shear failure, the average (or effective) stress level in the FRP reinforcement is much lower than its full tensile strength (Bousselham and Chaallal, 2008; Chen and Teng, 2003a, 2003b), regardless of the failure mode. Also, accurate evaluations of the FRP shear resistance can only be made if the orientation and shape of the shear crack are appropriately considered. For design use, the shear crack angle is commonly taken to be 45° from the beam longitudinal axis.

For RC beams strengthened with FRP full wraps, FRP rupture is the predominant failure mode (Chen and Teng, 2003b). When the FRP reinforcement is in the form of U-jackets or side strips, debonding of the FRP reinforcement from the concrete substrate generally governs the shear strength of the beam, and the evaluation of the shear resistance from the FRP becomes more challenging (Chen and Teng, 2003a). The present paper is concerned with the shear resistance contributed by FRP U-jackets or side strips in such a debonding failure.

Chen and Teng (2003a) presented a shear strength model for debonding failure, in which the bond performance between FRP and concrete is appropriately considered based on the work of Chen and Teng (2001a). This shear strength model is believed to be still the most advanced model available for the debonding failure mode based on the principle embodied in Equation 1 and a simple but rational representation of the debonding failure process. The model was shown to give close predictions for the shear contribution of FRP (Chen and Teng, 2003a). The model is based on the assumption that the shear resistance is governed by the development of a single critical shear crack that dominates the debonding failure process. For beams with a small shear span-to-depth ratio or with considerable steel shear reinforcement, significant secondary cracks are expected, but such secondary cracks are known to increase the bond performance between FRP and concrete. Therefore, the assumption of a single critical shear crack is conservative (Chen *et al.*, 2007; Teng *et al.*, 2006). In Chen and Teng's (2003a) model, there are two further assumptions.

(*a*) The bond strengths of all FRP strips intersected by the critical shear crack are fully mobilised at the ultimate state of beam shear failure. This is possible for FRP U-jackets, but unlikely for FRP side strips.
(*b*) The area of the bonded FRP on the beam sides contributing effectively to shear resistance has a triangular shape determined by the critical shear crack and the effective height of the FRP (Figure 1(a)). This assumption is conservative as it neglects the FRP between the compression face of the beam and the crack tip, and that within the concrete cover below the steel tension reinforcement for side bonded beams. A more accurate representation of the effective bonded area would be one which is trapezoidal in shape (Figure 1(b)).

Lu *et al.* (2009) presented results from a numerical study on the stress distribution in the FRP along the critical shear crack at debonding failure, based on the FRP-to-concrete bond–slip model of Lu *et al.* (2005). They showed that although the different shapes (i.e. different distributions of the crack width along the crack) assumed for the critical shear crack may result in significantly different stress distributions in the FRP, their effect on the stress distribution factor, defined as the ratio of the average to the maximum stress in the FRP reinforcement along the critical shear crack, is much less significant. They thus showed that Chen and Teng's (2003a) simple assumption for the stress distribution in the FRP leads to satisfactory predictions in most cases for the effective FRP stress factor. They also showed that the model of Chen and Teng (2003a) may be unconservative for beams with light steel tension reinforcement, but in practice shear failure is unlikely in such beams. For their computational model, they assumed that the slips between the FRP and the concrete immediately above and below the critical shear crack have the same magnitude but opposite directions (i.e. half of the crack width is accommodated by the slips in the portion of the FRP strip above the crack and half by those of the FRP strip below the crack). It should be noted that this assumption becomes unrealistic for the area around the crack tip (near the compression face of the beam) and that around the crack end (at the tension face of the beam) where the bond lengths of an FRP strip above and below the critical shear crack are very different. Lu *et al.*'s (2009) study did not examine the effect of different assumptions for the bonded area of FRP, the crack shapes employed in their numerical study were also less than realistic. Therefore, a more accurate computational model is needed for the assessment of the validity and accuracy of Chen and Teng's (2003a) model.

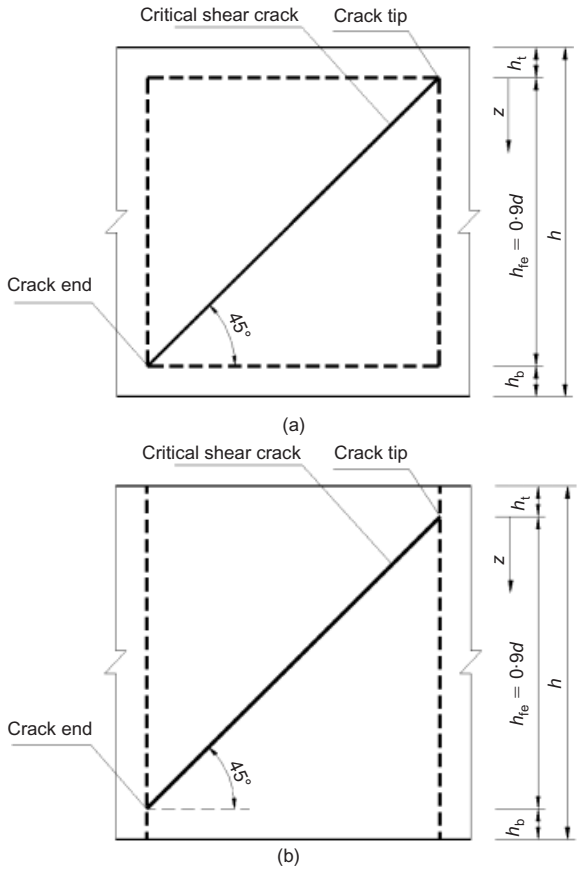

Figure 1. Bonded area of FRP: (a) idealised triangular bonded area of FRP (Chen and Teng, 2003a); (b) practical trapezoidal bonded area of FRP

The objectives of the present study are twofold. First, a theoretical model modified from Chen and Teng's (2003a) model through the adoption of a more accurate and realistic bonded area (Figure 1(b)) is presented. This modified model and the original model of Chen and Teng (2003a) are then both assessed using numerical results from a computational model, with particular attention to the effects of the two aforementioned assumptions of Chen and Teng (2003a). The computational model is similar but superior to that of Lu *et al.* (2009) in the following three aspects

(*a*) the assumption of equal slips immediately above and below the shear crack in Lu *et al.*'s (2009) model is no longer used
(*b*) a more realistic bonded area is included
(*c*) the possible crack shapes are more realistically represented using an appropriate crack shape function.

Chen and Teng's shear strength model

Chen and Teng (2001b, 2001c, 2003a, 2003b) were probably the first to propose the explicit inclusion of the effect of non-uniform stress distribution in the FRP on the shear capacity of FRP-strengthened RC beams. For such FRP reinforcement with fibres oriented at an angle β to the beam longitudinal axis, the FRP

contribution in Chen and Teng's (2003a, 2003b) model is given by

$$V_f = 2f_{f,e}t_f w_f \frac{h_{f,e}(\cot\theta + \cot\beta)\sin\beta}{s_f} \quad (2)$$

where θ is the critical shear crack angle; $h_{f,e}$ is the effective height of the FRP strips; w_f is the width of individual FRP strips; s_f is the centre-to-centre spacing of FRP strips along the beam longitudinal axis; and the effective FRP stress $\boldsymbol{f}_{f,e}$ is defined as the maximum FRP stress $\sigma_{f,max}$ times the stress distribution factor D_{frp}

$$\boldsymbol{f}_{f,e} = D_{frp}\sigma_{f,max} \quad (3)$$

For a shear debonding failure, the maximum FRP stress $\sigma_{f,max}$ is calculated as (Chen and Teng 2003a)

$$\sigma_{f,max} = \min\begin{cases} \boldsymbol{f}_{fu} \\ 0{\cdot}427\beta_L\beta_w\sqrt{\dfrac{E_f\sqrt{\boldsymbol{f}'_c}}{t_f}} \end{cases} \quad (4)$$

where

$$\beta_w = \sqrt{\frac{2 - w_f/(s_f\sin\beta)}{1 + w_f/(s_f\sin\beta)}} \quad (5)$$

$$\beta_L = \begin{cases} 1 & \text{if } \lambda \geqslant 1 \\ \sin\dfrac{\pi\lambda}{2} & \text{if } \lambda < 1 \end{cases} \quad (6)$$

and

$$\lambda = \frac{L_{max}}{L_e} \quad (7)$$

$$L_{max} = \begin{cases} \dfrac{h_{f,e}}{\sin\beta} & \text{for U-jackets} \\ \dfrac{h_{f,e}}{2\sin\beta} & \text{for side strips} \end{cases} \quad (8)$$

$$L_e = \sqrt{\frac{E_f t_f}{\sqrt{\boldsymbol{f}'_c}}} \quad (9)$$

in which $\boldsymbol{f}'_c$ (MPa) is the cylinder compressive strength of concrete; E_f (MPa) and $\boldsymbol{f}_{fu}$ (MPa) are the elastic modulus and the tensile strength of FRP respectively; t_f is the thickness of FRP strips, β_w is the strip width ratio factor, β_L is the bond length factor, λ is the normalised maximum bond length, and $h_{f,e}$ is the effective height of FRP, and L_{max} is the maximum value among the bond lengths of all the FRP strips intersected by the critical shear crack (i.e. the maximum bond length). The effective bond length L_e is that defined by Chen and Teng (2001a).

Assuming the full development of bond strength for all FRP strips intersected by the critical shear crack at the ultimate state of beam shear failure, Chen and Teng (2003a) showed that the stress distribution factor can be found from

$$D_{frp} = \begin{cases} \dfrac{2}{\pi\lambda}\dfrac{1 - \cos(\pi\lambda/2)}{\sin(\pi\lambda/2)} & \text{if } \lambda \leqslant 1 \\ 1 - \dfrac{\pi - 2}{\pi\lambda} & \text{if } \lambda > 1 \end{cases} \quad (10)$$

Equation 10 was derived and is exact for continuous FRP sheets, but for FRP strips the equation is approximate as the discrete strips need to be treated as smeared equivalent continuous sheets to arrive at the expression.

Modified shear strength model

As pointed out earlier, the bonded area between the FRP strips and the concrete is triangular in shape (Figure 1(a)) in the original model of Chen and Teng (2003a). A more accurate (and realistic) representation of the bonded area is one which is trapezoidal in shape, including a distance of h_t in the compression zone above the crack tip, and a distance of h_b in the tension zone below the steel tension reinforcement (Figure 1(b)). It should be noted that for beams bonded with FRP U-jackets, the lower beam corners are typically rounded for the installation of U-jackets. Since the bonded area below the shear crack does not affect the behaviour of a U-jacketed section, no consideration of the rounded corners is required in the modified shear strength model presented below.

As in Chen and Teng's (2003a) model, the stress distribution factor, D_{frp} is defined as

$$D_{frp} = \frac{\int_0^{h_{f,e}} \boldsymbol{\sigma}_{f,z}\,dz}{h_{f,e}\boldsymbol{\sigma}_{f,max}} \quad (11)$$

where $\boldsymbol{\sigma}_{f,z}$ is the stress in the FRP at the ultimate state at the location where the intersecting critical shear crack is at a vertical coordinate z (Figure 1(b)). It should be noted that in deriving Equation 11, it was assumed that discrete FRP strips can be treated as an equivalent FRP continuous sheet (2003a). Assuming that all the bonded strips intersected by the critical shear crack will develop their full bond strength at the ultimate state, $\boldsymbol{\sigma}_{f,z}$ is given by (Chen and Teng 2003a)

$$\boldsymbol{\sigma}_{f,z} = \min\begin{cases} \boldsymbol{f}_{fu} \\ 0{\cdot}427\beta_w\beta_{L,z}\sqrt{\dfrac{E_f\sqrt{\boldsymbol{f}'_c}}{t_f}} \end{cases} \quad (12)$$

where

$$\beta_{L,z} = \begin{cases} 1 & \text{if } \lambda_z \geqslant 1 \\ \sin\dfrac{\pi\lambda_z}{2} & \text{if } \lambda_z < 1 \end{cases} \quad (13)$$

For FRP side strips

$$\lambda_z = \begin{cases} \dfrac{(z+h_t)}{L_e \sin\beta} & 0 \leqslant z \leqslant \dfrac{h}{2} - h_t \\ \dfrac{(h_{f,e}+h_b-z)}{L_e \sin\beta} & \dfrac{h}{2} - h_t \leqslant z \leqslant h_{f,e} \end{cases} \quad (14)$$

and for FRP U-jackets

$$\lambda_z = \frac{(z+h_t)}{L_e \sin\beta} \quad (15)$$

The maximum stress in the FRP ($\boldsymbol{\sigma}_{f,max}$) can still be calculated using Equation 4, but the following actual maximum bond length should be used instead

$$L_{max} = \begin{cases} \dfrac{(h_{f,e}+h_t)}{\sin\beta} & \text{for U-jackets} \\ \dfrac{h}{2\sin\beta} & \text{for side strips} \end{cases} \quad (16)$$

Assuming that $\boldsymbol{\sigma}_{f,max} < \boldsymbol{f}_{fu}$, which is generally true, and that all the FRP strips intersected by the critical shear crack develop their full bond strength at the ultimate state, D_{frp} can be obtained by substituting Equations 12 to 16 into Equation 11. For FRP side strips:

$$D_{frp} = \begin{cases} \dfrac{2}{\pi\lambda_0}\dfrac{\cos(\pi\lambda_1/2)+\cos(\pi\lambda_2/2)-2\cos(\pi\lambda/2)}{\sin(\pi\lambda/2)} & \lambda_2 \leqslant \lambda \leqslant 1 \\ \dfrac{2}{\pi\lambda_0}\left(\cos\dfrac{\pi\lambda_1}{2}+\cos\dfrac{\pi\lambda_2}{2}\right)-\dfrac{2}{\lambda_0}+1+\dfrac{h_t+h_b}{h_{f.e}} & \lambda_1 < 1 < \lambda \text{ and } \lambda_2 < 1 < \lambda \\ \dfrac{2}{\pi\lambda_0}\cos\dfrac{\pi\lambda_2}{2}-\dfrac{1}{\lambda_0}+1+\dfrac{h_b}{h_{f,e}} & 1 \leqslant \lambda_1 \text{ and } \lambda_2 < 1 < \lambda \\ \dfrac{2}{\pi\lambda_0}\cos\dfrac{\pi\lambda_1}{2}-\dfrac{1}{\lambda_0}+1+\dfrac{h_t}{h_{f,e}} & 1 \leqslant \lambda_2 \text{ and } \lambda_1 < 1 < \lambda \\ 1 & 1 \leqslant \lambda_1 \text{ and } 1 \leqslant \lambda_2 \end{cases} \quad (17)$$

For FRP U-jackets

$$D_{frp} = \begin{cases} \dfrac{2}{\pi\lambda_0}\dfrac{\cos\dfrac{\pi\lambda_1}{2}-\cos\dfrac{\pi\lambda}{2}}{\sin\dfrac{\pi\lambda}{2}} & \lambda \leqslant 1 \\ \dfrac{2}{\pi\lambda_0}\cos\dfrac{\pi\lambda_1}{2}-\dfrac{1}{\lambda_0}+1+\dfrac{h_t}{h_{f,e}} & \lambda_1 \leqslant 1 \leqslant \lambda \\ 1 & 1 < \lambda_1 \end{cases} \quad (18)$$

where λ follows the definition of Equation 7 in which L_{max} is defined by Equation (16), and

$$\lambda_0 = \frac{h_{f,e}}{L_e \sin\beta} \quad (19)$$

$$\lambda_1 = \frac{h_t}{L_e \sin\beta} \quad (20)$$

$$\lambda_2 = \frac{h_b}{L_e \sin\beta} \quad (21)$$

It should be noted that in both Equations 17 and 18, $\lambda \geqslant \lambda_2$ is assumed because $\lambda < \lambda_2$ is very unlikely for beams of practical dimensions. The values of h_t can be taken as $0{\cdot}1d$ (Chen and Teng, 2003a). It should be noted that the modified model presented above reduces to the model of Chen and Teng (2003a) when $h_b = h_t = 0$.

Assuming $\boldsymbol{f}'_c = 30$ MPa, $E_f = 2{\cdot}3 \times 10^5$ MPa, $t_f = 0{\cdot}11$ mm and $h_{f,e} \geqslant h_b = 50$ mm, the calculated D_{frp} values from both the model of Chen and Teng (2003a) and the modified model are shown against λ in Figures 2(a) and 2(b) for FRP U-jackets and side strips respectively. The difference between the two models is small for U-jackets but is more significant for side strips (Figure 3). For both U-jackets and side strips, this difference reduces as the beam size increases (i.e. larger λ).

Finite-element modelling

Assumptions and general considerations

In order to evaluate the validity and accuracy of the two theoretical models (both Chen and Teng's (2003a)

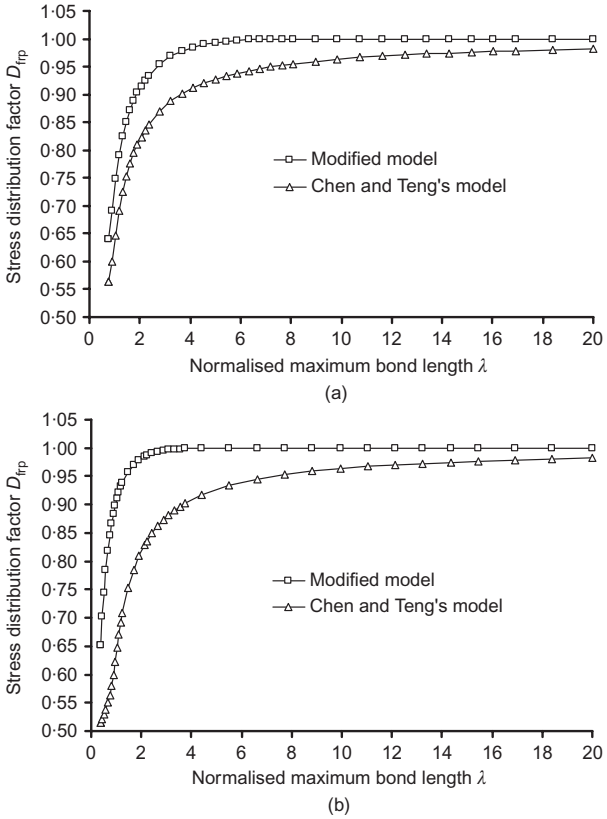

Figure 2. Stress distribution factor: (a) FRP U-jackets; (b) FRP side strips

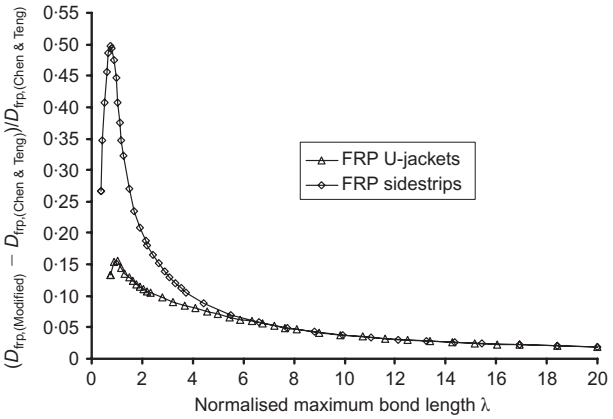

Figure 3. Difference in the stress distribution factor between the two theoretical models

original model and the modified model), a computational model was formulated and implemented using ABAQUS (ABAQUS 6.5, 2004). The computational model is based on the following assumptions

(*a*) the FRP strips are bonded to the entire height of the beam sides
(*b*) the distance from the tension face to the centroid of the steel tension reinforcement is 50 mm (Figure 4(a))
(*c*) the shear failure process is dominated by a single critical shear crack at an angle of 45° from the beam longitudinal axis. The effect of secondary shear cracks is conservatively ignored for reasons given earlier
(*d*) the tip of the critical shear crack at beam shear failure is located at a distance 0·1*d* from the compression face of the beam, while the crack end is located at the centre of the steel tension reinforcement (Figure 4(a)). Although the real shear crack is likely to extend to the tension face of the beam, this portion of the crack is not included for reasons given in Chen and Teng (2003a, 2003b).

Only a segment of the beam covering the horizontal projection of the critical shear crack within one quarter of the beam was modelled assuming a vertical plane of symmetry through the longitudinal axis of the beam (Figure 4). The critical shear crack was then discretised into a suitable number of divisions. The centrelines of the FRP strips were assumed to coincide with the centrelines of these divisions.

The computational representation of the interaction between the concrete and the FRP strips is shown schematically in Figure 4. To show the locations of the FRP strips clearly, the longitudinal steel bars are also included in Figures 4(a). For the present computational model, the concrete above and below the shear crack was assumed to be rigid; therefore all deformation in the model arises from the widening of the shear crack. Note that the elastic deformation of the concrete arising from the forces in the FRP strips can be easily taken

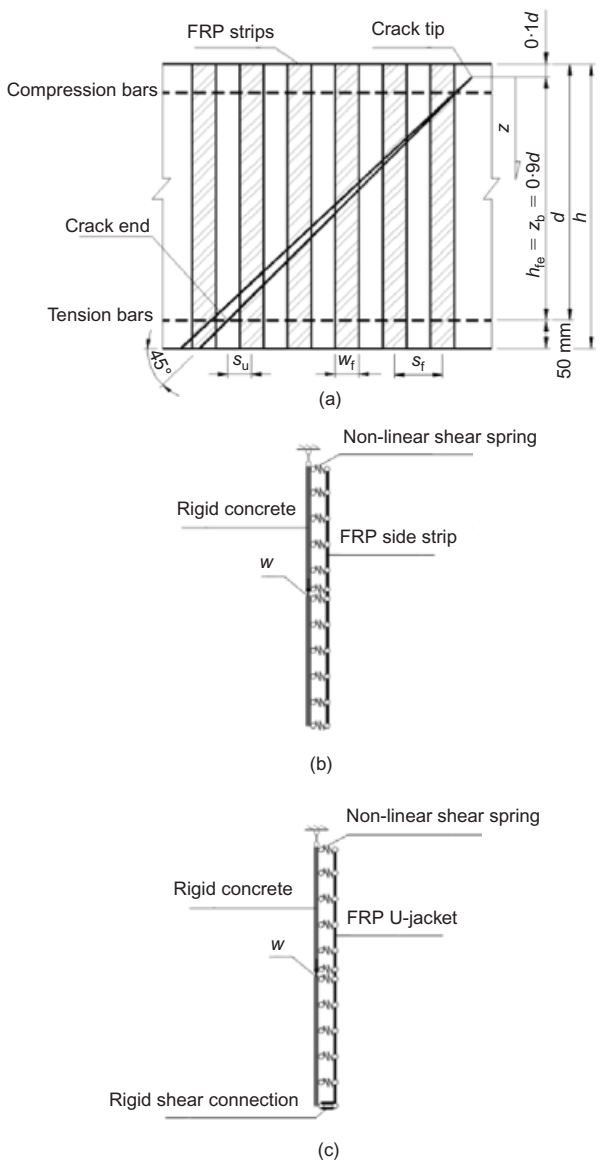

Figure 4. Computational model for RC beams shear-strengthened with FRP strips: (a) elevation ($s_{f,,1}$: spacing from the crack end to the centre of the first FRP strip; s_f: centre-to-centre spacing of FRP strips; w_f: width of individual FRP strips); (b) FRP side strips; (c) FRP U-jacket

into account in the present model, but numerical results showed that it has little effect on the results.

It should be noted that the distribution of the slips resulting from the widening of the shear crack is related to the bond–slip relationship and the bond lengths of the FRP strip above and below the shear crack, therefore the slips of the FRP strip relative to the concrete immediately above and below the crack are generally not the same, which is different from what was assumed by Lu *et al.* (2009). This is particularly true near the end and the tip of the crack because the bond lengths of an FRP strip on the two sides of the crack are very different.

Each FRP strip was modelled using a number of truss elements (element T2D2) as shown in Figures

4(b) and 4(c). Two vertical rigid bars, one above and one below the shear crack, were used to represent each division of the concrete substrate. The shear crack position in Figures 4(b) and 4(c) depends on the strip position relative to the shear crack in Figure 4(a). The crack width is denoted by w in Figures 4(b) and 4(c). The widening of the shear crack was simulated by prescribing a relative displacement (i.e. w) between the pair of rigid bars. The bond–slip relationship between concrete and FRP was simulated using shear springs (element SPRING2) connecting the nodes of truss elements representing the FRP strips to the rigid bars representing the concrete substrate. The properties of the shear springs were determined from the bond–slip model of Lu *et al.* (2005). For FRP U-jackets, the bottom end node of an FRP strip is fixed to the rigid concrete by a horizontal rigid bar (i.e. rigid shear connection). For FRP side strips, both the top and bottom end nodes are allowed to move.

Crack shape

A general shape function proposed by Chen and Teng (2003b) was adopted in this study to represent the shape of the critical shear crack. That is, the crack width w is described by

$$w = w_{\max} \times \begin{cases} \dfrac{1 - C\overline{z}}{1 - C}\overline{z} & 0 \leqslant C < \dfrac{1}{2} \\ 4C\overline{z}(1 - C\overline{z}) & \dfrac{1}{2} \leqslant C \leqslant 1 \end{cases} \qquad (22)$$

where the normalised vertical coordinate $\overline{z} = z/z_b$ with z and z_b being defined in Figure 4(a) and $w_{\max}$ is the maximum value of the crack width for a given crack (i.e. the maximum crack width). The shape of the crack varies with the shape parameter C (Figure 5). This function is thus capable of representing different crack shapes.

Bond–slip relationship

The bond–slip model for externally bonded FRP reinforcement proposed by Lu *et al.* (2005), which was shown to be the most accurate for modelling the bond–slip behaviour between FRP and concrete, was adopted in the present study (Figure 6(a)). The bond force $F_{b,f}$ in each shear spring between an FRP strip and the concrete can be found from

$$F_{b,f} = w_f \times l_f \times \tau_f \qquad (23)$$

where w_f is the width of the FRP strip, l_f is the length of the FRP truss element and τ_f is the bond shear stress. The equations associated with the bond–slip model of Lu *et al.* (2005) are shown in Figure 6 for completeness. Figure 6 also shows the predicted bond–slip curve for the case of $f'_c = 30$ MPa and $w_f/s_f = 1{\cdot}0$.

Mesh convergence: truss element size

The following material properties were used in all the numerical simulations reported in this paper unless stated otherwise: concrete cylinder compressive strength $f'_c = 30$ MPa (with an equivalent cube strength of 37 MPa (CEB–FIP, 1993)); concrete tensile strength $f_t = 0{\cdot}395 f_{cu}{}^{0{\cdot}55}$ (GB-50010, 2002); FRP thickness $t_f = 0{\cdot}11$ mm; elastic modulus of FRP $E_f = 2{\cdot}3 \times 10^5$ MPa; and tensile strength of FRP $f_f = 3900$ MPa. The beam had a height such that $h_{f,e} = 300$ mm, unless otherwise stated. The beam considered had its sides fully covered by continuous FRP sheets with vertically oriented fibres only. The use of continuous FRP sheets is consistent with the derivation of the theoretical models and also simplifies the discussions. Such a continuous FRP sheet is equivalent to and was modelled as a number of FRP strips with the strip width w_f being the same as the strip spacing s_f, and with the spacing from the crack end to the centre of the first FRP strip $s_{f,1} = s_f/2$ (Figure 4). The number of strips to be used to represent such a continuous sheet was determined from a mesh convergence study.

All the truss elements had the same length for ease of modelling and the shear crack position and/or the strip length were appropriately rounded to suit the element size. A convergence study was conducted for the truss element size using a single-strip model with the crack opening displacement applied at the middle of

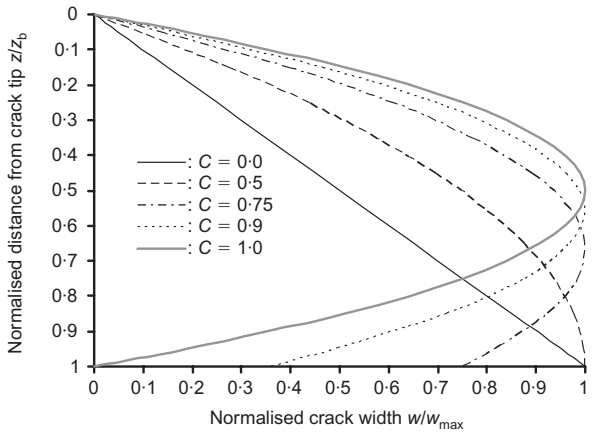

Figure 5. Crack shapes corresponding to different values of C (Chen and Teng, 2003b)

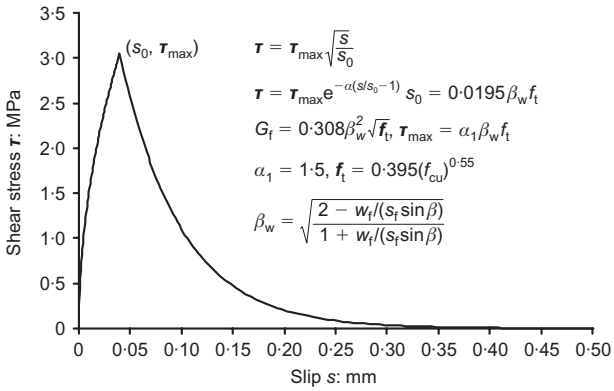

Figure 6. Lu et al.'s FRP-to-concrete bond–slip relationship for $f'_c = 30$ MPa and $w_f/s_f = 1{\cdot}0$

the strip. Results of two simulations with 1 mm and 2 mm element sizes (Figure 7(a)) are nearly identical. The predicted maximum stress value in FRP (Figure 7(a)) is 1048 MPa, which in close agreement with a value of 1045 MPa calculated from the corresponding bond strength model of Lu *et al.* (2005), showing the accuracy of the computation model. A truss element size of 1 mm was adopted in all subsequent numerical simulations of the study. Note that Chen and Teng's (2001a) bond strength model employed in the shear strength model of Chen and Teng (2003a) and the present modified shear strength model predicts a closely similar value of 1022 MPa. Chen and Teng's (2001a) bond strength model was recommended by Lu *et al.* (2005) following an exhaustive study for design use due to its simplicity and accuracy.

Mesh convergence: spacing of the FRP strips

In the interest of computational efficiency and to verify the convergence of the model, numerical simulations were also conducted to determine the appropriate number (or the appropriate spacing) of discrete FRP strips to represent a continuous FRP sheet with vertical fibres ($s_f = w_f$). Figure 7(b) shows the development of the effective stress in the FRP strips with the maximum crack width (i.e. w_{max}) for different values of FRP strip spacing (s_f). When the FRP strip spacing s_f is large (e.g. $s_f = h_{f,e}/5$), the stepwise drop of the effective stress due to the complete debonding of individual strips in the descending branch of the curve is also large. As s_f decreases, such drops become smaller. Figure 7(b) clearly shows the trend that the 'ideal' value of effective stress for a continuous FRP sheet lies at the midpoint of each stepwise drop. With $s_f = h_{f,e}/20$, the magnitude of the drops compared to the deduced value for a continuous FRP sheet ($s_f = 0$) is about 2·5%. This is because when $s_f = h_{f,e}/20$, the corresponding value for each step drop is about $1/20 = 5\%$ of the effective stress of the FRP sheet, and half of the step drop is around 2·5%. Based on the above observations, in this study $s_f = h_{f,e}/20$ was adopted to closely represent the shear resistance contribution of a continuous FRP sheet.

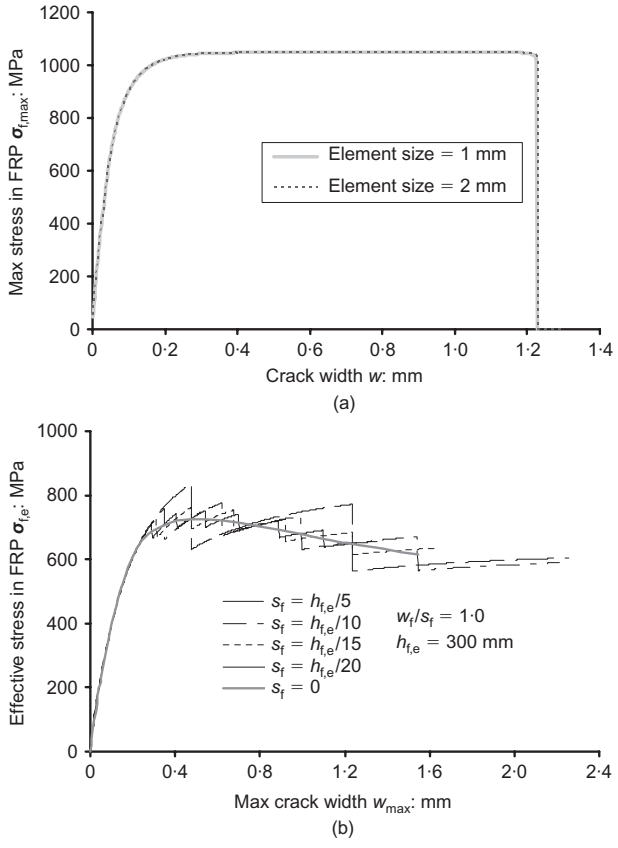

Figure 7. Mesh convergence: (a) effect of truss element size predicted by a single strip model; (b) effect of spacing of FRP strips (C = 0)

Performance of the two theoretical models

To assess the performance of Chen and Teng's (2003a) theoretical model and the modified model presented in this paper quantitatively , the following factor is defined

$$K_f = \sigma_{f,e} / f_{f,e} \quad (24)$$

where K_f is referred to as the mobilisation factor of the FRP strips, $\sigma_{f,e}$ is the average stress (or effective stress) of the FRP strips intersected by the critical shear crack obtained from a numerical simulation, and $f_{f,e}$ is the effective stress in the FRP from either of the two theoretical models.

It should be noted that in both theoretical models, the value of $f_{f,e}$ is based on the assumption that all the FRP strips intersected by the critical shear crack develop their full bond strengths at the shear failure of the beam. This assumption is not made in the computational model. In addition, the shape of the crack, representing the distribution the crack width, can be varied in the computational model. Clearly the computational model depicts more accurately the stress development in FRP strips and hence the shear contribution of the FRP than the two theoretical models. In this section, the accuracy of the theoretical models is assessed in terms of the mobilisation factor defined above.

Figure 8 shows that the value of K_f for FRP side strips increases as the crack widens and then decreases as the strips debond in a sequential manner. For Chen and Teng's (2003a) model (Figure 8(a)), the maximum value of K_f reached before the commencement of debonding is around one for values of C from 0·25 to 0·75, which covers the range of crack shapes most likely to be found in practice. Therefore it can be said that Chen and Teng's (2003a) model is accurate in predicting the shear resistance of FRP side strips. The maximum K_f value is larger than 1·0 (conservative) for larger C values and smaller than 1·0 (unconservative) for smaller C values. By contrast, the modified theoretical model leads to

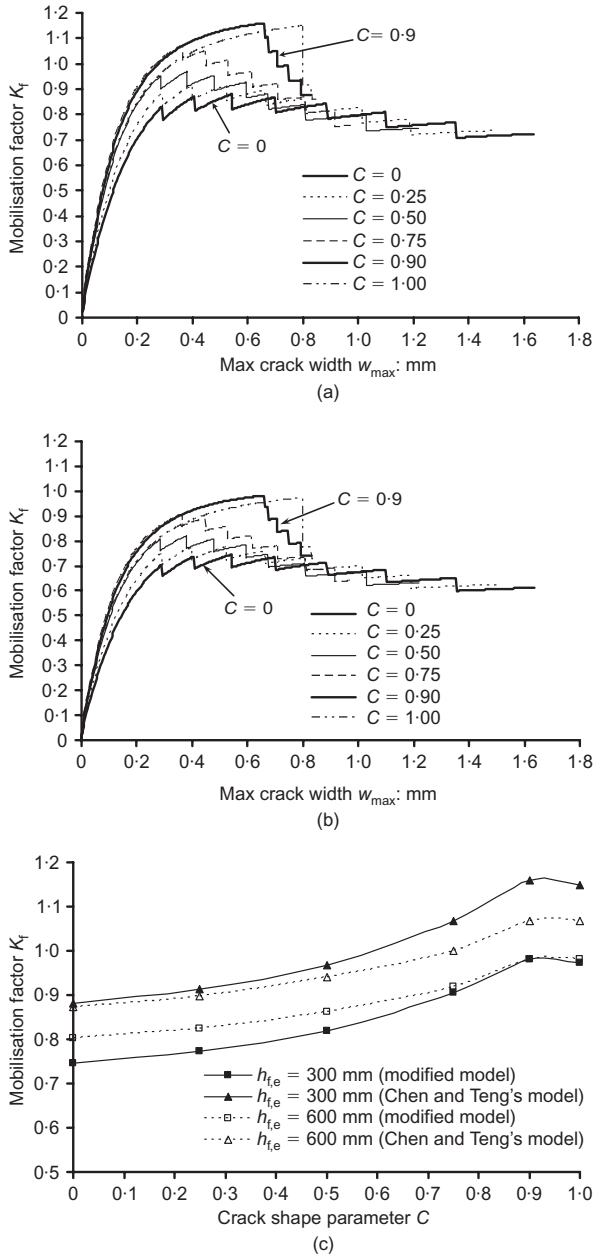

Figure 8. Values of K_f for FRP side strips: (a) K_f of Chen and Teng's (2003a) model ($h_{f,e} = 300$ mm); (b) K_f of the modified shear strength model ($h_{f,e} = 300$ mm); (c) maximum value of K_f

unconservative predictions for the common range of crack shapes (Figure 8(b)). The crack shape with $C = 0$ is the most critical throughout the development process of shear resistance for both models.

Figure 8(c) shows the maximum K_f value against the crack shape parameter C for both models and two practical beam sizes. From the figure it can be seen that K_f generally increases with C for both models. Chen and Teng's (2003a) model is nearly independent of the beam size when C is small but becomes more conservative for the small beam when C is large. The modified model is unconservative for all C values. It is more unconservative for the small beam when C is small but the accuracy becomes almost the same for both beam sizes when C approaches 1·0. Overall, Chen and Teng's (2003a) original model gives better and more conservative predictions than the modified model.

In a similar fashion, the numerical results for FRP U-jackets are presented in Figure 9. In general, the mobilisation factor increases for both models when the crack shape becomes more symmetrical (i.e. C approaches 1·0) (Figures 9(a) and 9(b)). Figure 9(c) shows the effect of the crack shape parameter C on the maximum K_f value. The predictions of the computational model are seen to closely match the predictions of both theoretical models (i.e. K_f is close to 1 in all

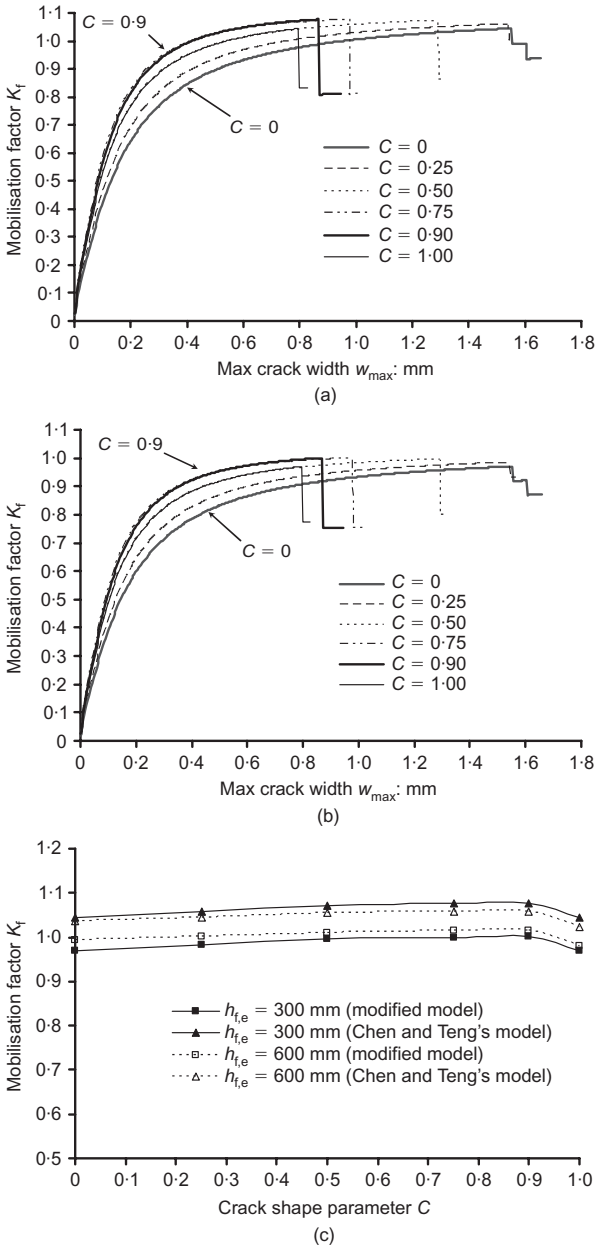

Figure 9. Values of K_f for FRP U-jackets: (a) K_f of Chen and Teng's (2003a) model ($h_{f,e} = 300$ mm); (b) K_f of the modified shear strength model ($h_{f,e} = 300$ mm); (c) maximum value of K_f

cases) (Figure 9(c)). Figure 9(c) also shows that for FRP U-jackets, the FRP shear contribution is much less sensitive to the crack shape compared to FRP side strips (Figure 8(c)). For the crack shapes examined in this study and for a beam with $h_{f,e} = 300$ mm, the maximum difference between the computational model and Chen and Teng's (2003a) model occurs when the crack shape is nearly symmetrical ($C = 0{\cdot}9$) and Chen and Teng's (2003a) model is conservative by 8·0%. This difference is reduced when the beam size increases. The modified theoretical model gives accurate predictions over the full range of crack shapes for the two different beam heights, with the maximum difference being less than 3·0%.

Both theoretical models are based on the unconservative assumption that all FRP strips reach their full bond strength at beam failure owing to debonding. In Chen and Teng's (2003a) original model, the bonded FRP areas between the compression face of the beam and the crack tip and covering the tensile concrete cover are conservatively neglected, which counterbalances the effect of the assumption of full bond strength development. This counterbalancing effect is not available in the modified model, which is based on a more accurate representation of the bonded area. As a result, Chen and Teng's (2003a) original model gives more conservative predictions than the modified model. This counterbalancing effect is more significant for FRP side strips than for FRP U-jackets because for a given beam size, FRP side strips have shorter bond lengths than a corresponding configuration of FRP U-jackets. Therefore, for FRP side strips, the original model is much more accurate while the modified model can be significantly unconservative.

Conclusion

This paper has been concerned with the evaluation of the shear resistance contributed by externally bonded FRP reinforcement in RC beams shear-strengthened with FRP U-jackets or side strips; such beams typically fail by the debonding of the FRP reinforcement from the concrete substrate. In this paper, a theoretical shear strength model in closed-form expressions modified from a model proposed by Chen and Teng (2003a) for shear debonding failure was presented. The predictions of both the original model of Chen and Teng and the modified theoretical model were then compared with results from a computational model that does not make use of several restrictive assumptions adopted by the two theoretical models. With the results from the computational model taken as the accurate reference values, the numerical results and discussions presented in the paper allow the following conclusions to be made about the two theoretical models

(*a*) both Chen and Teng's (2003a) original model and the modified model lead to reasonably accurate predictions for the shear resistance of externally bonded FRP reinforcement (both FRP U-jackets and side strips) for the practical range of crack shapes

(*b*) the accuracy of both models increases as the beam height increases

(*c*) for both FRP U-jackets and side strips, Chen and Teng's (2003a) original model leads to more conservative predictions than the modified model for all the crack shapes examined

(*d*) for FRP U-jackets, both Chen and Teng's (2003a) original model and the modified model provide very close predictions, with the modified model being slightly more accurate. For FRP side strips, Chen and Teng's (2003a) original model provides more accurate predictions than the modified model

(*e*) the original model of Chen and Teng (2003a) is more suitable for use in design given its overall accuracy and simpler form.

Acknowledgements

The authors are grateful for the financial support received from the Research Grants Council of the Hong Kong SAR (project no.: PolyU 5151/03E) and The Hong Kong Polytechnic University provided (project code: BBZH). They would also like to acknowledge the support from the Scottish Funding Council for the Joint Research Institute between the University of Edinburgh and Heriot-Watt University which forms part of the Edinburgh Research Partnership in Engineering and Mathematics (ERPem). Thanks are also due to Dr O. Rosenboom for the assistance offered by him during the preparation of this paper.

References

ABAQUS 6.5 (2004) *ABAQUS Analysis User's Manual*. ABAQUS, Providence.

Bousselham A and Chaallal O (2004) Shear strengthening reinforced concrete beams with fiber-reinforced polymer: assessment of influencing parameters and required research. *ACI Structural Journal* **101(2)**: 219–227.

Bousselham A and Chaallal O (2006) Behavior of RC T beams strengthened in shear with CFRP: an experimental study. *ACI Structural Journal* **103(3)**: 339–347.

Bousselham A and Chaallal O (2008) Mechanisms of shear resisitance of concrete beams strengthened in shear with externally bonded FRP. *Journal of Composites for Construction*, ASCE **12(5)**: 499–512.

Cao SY, Chen JF, Teng JG, Hao Z and Chen J (2005) Debonding in RC beams shear strengthened with complete FRP wraps. *Journal of Composites for Construction, ASCE* **9(5)**: 417–428.

Carolin A and Taljsten B (2005a) Experimental study of strengthening for increased shear bearing capacity. *Journal of Composites for Construction, ASCE* **9(6)**: 488–496.

Carolin A. and Taljsten B (2005b) Theoretical study of strengthening for increased shear bearing capacity. *Journal of Composites for Construction, ASCE* **9(6)**: 497–506.

CEB–FIP (1993) *CEB–FIP Model Code 1990*. Thomas Telford, London, UK.

Chaallal O, Nollet MJ and Perraton D (1998) Strengthening of reinforced concrete beams with externally bonded fibre-reinforced-plastic plates: design guidelines for shear and flexure. *Canadian Journal of Civil Engineering* **25(4)**: 692–704.

Chen JF and Teng JG (2001a) Anchorage strength models for FRP and steel plates bonded to concrete. *Journal of Structural Engineering, ASCE* **127(7)**: 784–791.

Chen JF and Teng JG (2001b) Shear strengthening of RC beams by external bonding of FRP composites: a new model for FRP debonding failure. *Proceedings 9th International Conference on Structural Faults and Repairs, London*, UK. CD-ROM.

Chen JF and Teng JG (2001c) A shear strength model for FRP strengthened RC beams. *FRPRCS-5: Fibre-reinforced Plastics for Reinforced Concrete Structures, Cambridge* **1**, 205–214.

Chen JF and Teng JG (2003a) Shear capacity of FRP-strengthened RC beams: FRP debonding. *Construction and Building Materials* **17(1)**: 27–41.

Chen JF and Teng JG (2003b) Shear capacity of FRP strengthened RC beams: fibre reinforced polymer rupture. *Journal of Structural Engineering, ASCE* **129(5)**: 615–625.

Chen JF, Yuan H and Teng JG (2007) . *Engineering Structures* **29(2)**: 259–270.

Colotti V, Spadea G and Swamy RN (2004) Analytical model to evaluate failure behavior of plated reinforced concrete beams strengthened for shear. *ACI Structural Journal* **101(6)**: 755–764.

Deniaud C and Cheng JJR (2004) Simplified shear design method for concrete beams strengthened with fiber reinforced polymer sheets. *Journal of Composites for Construction, ASCE* **8(5)**: 425–433.

GB-50010 (2002) *Code for Design of Concrete Structures*. China Architecture and Building Press, Beijing, China. (In Chinese).

Hollaway LC and Teng JG (2008) *Strengthening and Rehabilitation of Civil Infrastructures Using Fibre-Reinforced Polymer (FRP) Composites*. Woodhead Publishing Limited, Cambridge.

Khalifa A, Gold WJ, Nanni A and Aziz A (1998) Contribution of externally bonded FRP to shear capacity of RC flexural members. *Journal of Composites for Construction, ASCE* **2(4)**: 195–203.

Khalifa A and Nanni A (2002) Rehabilitation of rectangular simply supported RC beams with shear deficiencies using CFRP composites. *Construction and Building Materials* **16(3)**: 135–146.

Leung CKY, Chen Z, Lee S, Ng M, Xu M and Tang J (2007) Effect of size on the failure of geometrically similar concrete beams strengthened in shear with FRP strips. *Journal of Composites for Construction, ASCE* **11(5)**: 487–496.

Li A, Diagana C and Delmas Y (2002) Shear strengthening effect by bonded composite fabrics on RC beams. *Composites, Part B* **33(3)**: 225–239.

Lu XZ, Chen JF, Ye LP, Teng JG and Rotter JM (2009) RC beams shear-strengthened with FRP: stress distributions in the FRP reinforcement. *Construction and Building Materials* **23(4)**: 1544–1554.

Lu XZ, Teng JG, Ye LP and Jiang JJ (2005) Bond–slip models for FRP sheets/plates bonded to concrete. *Engineering Structures* **27(6)**: 381–389.

Taljsten B (2003) Strengthening concrete beams for shear with CFRP sheets. *Construction and Building Materials* **17(1)**: 15–26.

Teng JG, Chen JF, Simth ST and Lam L (2002) *FRP-strengthened RC Structures*. Wiley, Chichester.

Teng JG, Chen GM, Chen JF, Rosenboom OA and Lam L (2009) Behavior of RC beams shear strengthened with bonded or unbonded FRP wraps. *Journal of Composites for Construction, ASCE* **13(5)**: 394–404.

Teng JG, Lam L and Chen JF (2004) Shear strengthening of RC beams using FRP composites. *Progress in Structural Engineering and Materials* **6(3)**: 173–184.

Teng JG, Yuan H and Chen JF (2006) FRP-to-concrete interfaces between two adjacent cracks: Theoretical model for debonding failure. *International Journal of Solids and Structures* **43(18–19)**: 5750–5778.

Triantafillou TC (1998) Shear strengthening of reinforced concrete beams using epoxy-bonded FRP composites. *ACI Structural Journal* **95(2)**: 107–115.

Triantafillou TC and Antonopoulos CP (2000) Design of concrete flexural members strengthened in shear with FRP. *Journal of Composites for Construction, ASCE* **4(4)**: 198–205.

Discussion contributions on this paper should reach the editor by 1 October 2010